Chains of Artificial Atoms in a Magnetic Field

J. G. Díaz and J. Planelles*

Departament de Ciències Experimentals, UJI, Box 224, E-12080 Castelló, Spain

Received: September 24, 2003; In Final Form: January 9, 2004

The energy structure of one-dimensional chains of spherical nanocrystals is investigated. Both, uniform and multilayer nanocrystals are studied. Calculations are performed with the **k·p** method and the envelope function approximation (EFA). The valence subband mixing is accounted for by considering a four-band Hamiltonian. The high (spherical) symmetry of the building blocks leads to a unique energy structure with miniband widths depending on the *z*-component of the angular momentum. These minibands are $(2L + 1)$ quasi-degenerated in the low-coupling regime, L being the quantum number of the angular momentum. The magnetic field splits quasidegeneracy leading to a mixture of successive narrow and wide minibands. The ground miniband of chains built of antidots becomes very narrow in the strong coupling regime and separates from the rest of the spectrum, so that a strong luminescence red-shift is predicted.

1. Introduction

Vertically correlated quantum dots, referred to as a quantum dot superlattice,[1−6] exhibit a strong electronic coupling with unique properties.[7,8] The self-assembly driving force in these structures may come from strain fields, as is the case in the Stranski-Krastanow (SK) growth technique, that basically consists of the sequential deposition of a material onto a substrate that is lattice mismatched to it, yielding a vertical self-organized growth of coherent islands of the deposited material.[9−17] Different shapes, including pyramids,[9−11] truncated pyramids,[12−15] and lens,[16,17] have been used to theoretically model the properties of these vertically coupled quantum dots structures (VCQDs) leading in all cases to a similar ordering and density distribution (close to the base of the pyramid-like dots) of the low-lying electron and hole states.

Self-assembled nanocrystals, with promising potential applications in the fields of communications (multi-qbits gates,[18−20] terahertz detectors[21,22]), optics (photodetectors[23] and lasers[24]), and biomedical imaging,[25] can also be obtained by means of wet chemistry methods, i.e., by colloidal growth of free-standing nanocrystals. Wet chemistry methods allow not only the synthesis of uniform spherical nanocrystals but also the fabrication of multishell structures made up of concentric layers with sizes and compositions highly controlled during the synthesis.[26−34] Unlike the SK-grown quantum dots (QDs), these nanocrystals, with nearly spherical shape, lead to atomic-like symmetries and degeneracies for the energy states.[29] Since spheres are symmetric in every respect, these QDs naturally have a strong tendency to closely pack, resulting in tridimensional (3D) arrays.[35−38] However, depending on experimental conditions, lower dimensional superlattices can be also obtained.[35] Thus, large wires composed of metal nanoparticles[39,40] or finite chains of silica microspheres[41] have been observed. We must stress at this point that real QDs superlattices result from two opposite forces: disorder and interdot coupling. Current wet-chemistry methods provide size distributions of less than 5%, and formation of states across a dense array of dots have been pointed out as responsible for changes in the optical spectra when QDs aggregate.[42,43] Theoretical calculations on QDs chains show that up to 2% size fluctuations all states remain delocalized, when fluctuations reach 5% some states become localized, and beyond 10% almost no delocalization occur.[44]

In this paper we complete our previous study on the formation of electron minibands in 1D chains of uniform CdS and two-layered ZnS/CdS antidot systems,[44] and extend it to the corresponding hole minibands. Hereafter we will refer to this kind of two-layer nanocrystals, with an external clad having a narrower band gap than the internal core and therefore acting as a well for the density charge, as antidots. Additionally, a detailed study of 1D arrays of uniform InAs and two-layered ZnSe/InAs antidots, materials with very different effective masses and band offsets, is carried out. The aim of the study is 2-fold: (1) to examine to what extent some singular properties of previously studied 1D array of spherical quantum dots[44] are linked to shape or to specific characteristics (effective mass, band offsets, etc.) of the building block material, (2) to extend the study to the, a priori more complex, valence band. To our knowledge, no experimental realization of these "wires" has been done yet (although rodlike structures built of several closely ordered semiconductor nanocrystals have been already observed[45]). Nevertheless, it is important to put forward the collective properties of these close-packed 1D arrays of QDs for many possible device applications. One should expect significant differences in ordering and density distribution of low-lying electron and hole states of the VCQDs grown by wet-chemistry methods and those grown by the above-mentioned SK technique, because we may qualitatively relate all the states of truncated pyramids and lenses to just the $(L + M_z)$ odd states of a sphere (L, M_z are the quantum numbers of total angular momentum and its *z*-component, respectively). In fact, calculations on the electronic structure of an infinite 1D array of vertically coupled InAs truncated pyramids embedded in GaAs matrix reveal that the succesive electron minibandwidths are almost identical,[15] while a similar study on the 1D array of spherical CdS nanodots shows a strong dependence of minibandwidths on M_z.[44]

* Corresponding author. E-mail: planelle@exp.uji.es.

10.1021/jp0368536 CCC: $27.50
Published on Web 02/07/2004

The effect of an external magnetic field on these structures is also investigated. The study of magnetic field effects on semiconductor quantum dots is of interest for two reasons. First the quantum confinement is weaker and the electron effective mass lighter than in atomic physics, which allows us to observe effects that for natural atoms would require magnetic fields many orders of magnitude stronger than those accessible in the laboratory.[46−51] Second, such investigations are also of practical interest since magnetic fields can be used to tune quantum dot lasers and other optical nanodevices[52−55] or to manipulate the tunnel barrier between coupled dots.[56,57] In section 3.2 of this paper we will show that, in particular, the magnetic field enhances interdot tunneling.

The calculations are performed within the effective mass approximation. The valence subband mixing is accounted for by means of a four-band Hamiltonian for the hole states. The simple labeling of the energy states in accordance with the global (envelope) symmetries of the nanodots provided by the effective mass model (EMM) and the envelope function approximation (EFA), as well as the easy account for the effects of external fields, makes this method especially suitable for the purposes of the paper. The agreement of the continuum EMM-EFA approach and the atomistic tight-binding (TB) theory in this kind of studies has been stated elsewhere.[44,58]

2. Theory and Computational Details

Linear systems of nanocrystals—with or without magnetic field $\mathbf{B} = (0,0,B)$—exhibit axial symmetry. Thus, calculations in the EMM approach have been performed in cylindrical coordinates (ρ, z). The corresponding one-band effective mass equation for describing the electrons of the conduction-band[59] is given by

$$\left(-\frac{1}{2m^*}\Delta + \frac{B^2}{8m^*}\rho^2 + \frac{BM_z}{2m^*} + V(\rho, z) - E_{n,M_z}\right)\Phi_{n,M_z} = 0 \quad (1)$$

where m^* is the effective mass, V is the confining potential formed by the band offsets (the polymeric environment is modeled by a high, 4 eV, barrier), and $M_z = 0, \pm 1, \pm 2, ...$ is the quantum number of the projection of the angular momentum $\mathbf{L}$ onto the magnetic field (B) axis. Because of the axial symmetry of the system, the electron states are labeled by M_z. But, for comparison with the spherically symmetric states of a single quantum dot, in the limit of low coupling regime, we additionally use the notation $\tilde{n}L$, where $\tilde{n}$ labels the consecutive states of a given spherical symmetry L.

For the proper description of the valence band states, the valence subband mixing has to be taken into account. Since we are interested in the energies near the top of the valence band, where the split-off part in the mixed hole states is negligible, and the heavy-hole and light-hole zone center states govern the electronic structure, the four-band $\mathbf{k}\cdot\mathbf{p}$ Hamiltonian[60] has been employed. Transforming the Hamiltonian from Cartesian to cylindrical coordinates (ρ, z, ϕ) and integrating over the ϕ angle leads to four coupled differential equations for the envelope function components $f^i_{F_z}(\rho, z)$.[61,62] This Hamiltonian commutes only with the operator $\mathbf{F}_z$ of the projection of the total angular momentum $\mathbf{F} = \mathbf{L} + \mathbf{J}$ onto the field axis ($\mathbf{J}$ is the Bloch angular momentum ($J = 3/2$) and $\mathbf{L}$ is the envelope angular momentum). In the limit of low coupling regime, the states can be labeled by the spherical notation $(\tilde{n}Q_F, F_z)$ of a single quantum dot, where Q denotes the spectroscopic notation for the lowest value of the envelope angular momentum L for a given F,[63] and $\tilde{n}$ labels consecutive states of a given symmetry. Finally, according to ref 64, the interaction with an external uniform magnetic field is only included in the diagonal elements of the four-band $\mathbf{k}\cdot\mathbf{p}$ Hamiltonian ($\mathscr{H}_{ex}$ in ref 64).

The electron and hole equations have been solved numerically using the finite-differences (FD) method on a rectangular two-dimensional grid (ρ, z) defined from $[0, -z_{max}]$ up to $[\rho_{max}, z_{max}]$. The discretization of these differential equations yields eigenvalue problems of asymmetric huge and sparse matrixes H_{FD} that have been solved by employing the iterative Arnoldi factorizations[65] implemented in the ARPACK package.[66]

Boundary conditions (BCs) for nonperiodic systems are: $\chi(\rho, -z_{max}) = \chi(\rho, z_{max}) = \chi(\rho_{max}, z) = \chi(0, z) = 0$ (for $M_z = 0$ states $(\partial\chi/\partial\rho)_{(0,z)} = 0$ replaces $\chi(0, z) = 0$). In the above equation χ represents either the electron or a hole envelope function component. Infinite 1D chains of nanocrystals are periodic in the z-axis, then, BCs $\chi(\rho, -z_{max}) = \chi(\rho, z_{max}) = 0$ are replaced by $\chi(\rho, z + D) = e^{iqD}\chi(\rho, z)$, where D is the superlattice constant and $0 < q < \pi/D$. The minibands dispersions $E(q)$ are obtained by diagonalizing complex, sparse, and huge $H_{FD}(q)$ matrixes for different values of q within the above-mentioned range. For $q = 0$ and $q = \pi/D$ we get the electron minibands limits. It is not the case in the valence band, where the HH-LH interaction may lead the minibands limits to appear at other q-values.

No strain effects are included in our calculations since, on one hand, the nanocrystals considered are surrounded by a polymeric solution and, on the other hand, in the studied antidots (where two different semiconductors are matching) the well-acting layer is just a few monolayers thick and should relax to the lattice constant of the core.

We have checked nonparabolicity effects on the QD building blocks of the studied 1D chains in a magnetic field. No essential different results are achieved, according to refs 67,68 where it is concluded that the parabolic band approximation is applicable to dots with a large radius, as those studied here.

Finally, since in multilayer nanocrystals the electronic density is mainly concentrated in the well-acting layer, the effective mass and Luttinger parameters of this layer are used in the entire structure.

3. Results and Discussion

3.1. Electron Minibands. We have performed calculations for two different 1D chains, namely, spherical uniform InAs, which resemble tightly bound core electron systems, and ZnSe/InAs nanocrystals, with the electronic density mainly concentrated in the outer shell. As stated above, we choose this multishell system because its constitutive materials have very different effective masses and band offsets. The noncrystalline environment of the QDs (solvents or glass matrixes) is modeled by a 4-eV rectangular barrier and the InAs effective mass employed is $m^* = 0.024$.[69] The system of minibands for a chain built of $R = 8$ nm radius InAs nanocrystals both in the absence and in the presence (20 T) of an external magnetic field is shown in Figure 1. Minibands in Figure 1a evolve from the $(2L + 1)$-fold degenerate single dot electron energy spectrum that can still be seen in the limit of weak coupling regime that corresponds to an interdot distance $d \geq 1.5$ nm.[70,71] Although the effective mass, lighter than in CdS, reduces, on one hand, the closeness of the states and, on the other hand, leads to nonnegligible bandwidths for larger distances, the main trends observed in the previously studied uniform CdS system[44] are also obtained here. Namely, as can be seen in Figure 1, the width of the minibands is larger for higher and more diffused

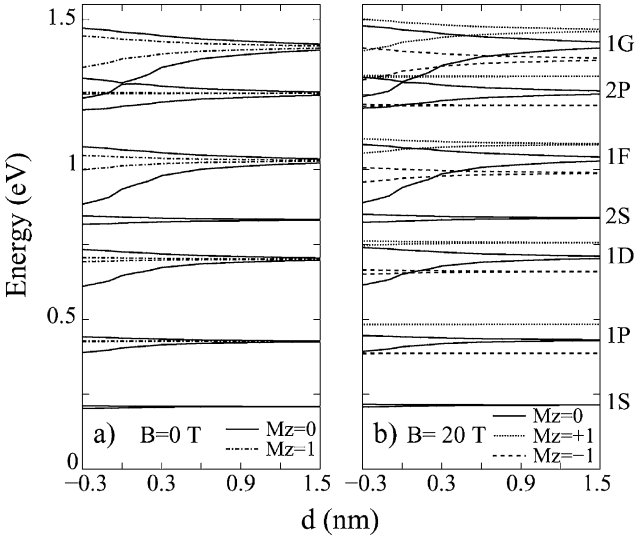

Figure 1. $M_z = 0, \pm 1$ electron minibands edges for a chain built of $R = 8$ nm InAs nanocrystals vs interdot separation distance d. Distance $d = 0$ corresponds to touching dots, $d = -0.6$ nm represents a dots overlap of about a lattice constant. (a) Magnetic field $B = 0$ T; (b) Magnetic field $B = 20$ T.

states and decreases as the value of $|M_z|$ increases, mainly originated from the fact that minibands coming from states with higher $|M_z|$ do not build density probability along the z-axis.

These general trends are, though, quite different from those observed when SK QDs couple to form a chain. In these systems, successive minibands show similar widths and overlap for a given interaction distance, producing a continuum of energy.[15] We have also carried out calculations on a chain of unstrained truncated cones with the same hight/base ratio and materials (InAs embedded in a GaAs matrix) as the truncated pyramids reported in ref 15, and have obtained similar results, i.e., successive minibands with different M_z values show similar widths, almost independent of M_z, and these bandwidths lead to an overlap for a given interaction distance, also producing a continuum of energy.

These differences mainly originate from the shape of the chain building blocks. Thus, states of truncated pyramids and lenses may be qualitatively related to the $(L + M_z)$ odd states of a sphere. Then, on one hand, the $(2L + 1)$ degeneracy reduces to L in an ideal hemisphere (in a real nanocrystal the L states are close but nondegenerate[14]). On the other hand, our calculations reveal (Figure 1a) that only $M_z = 0$ minibands open significantly to overlap (see, e.g., the 2P and 1G minibands in Figure 1a). However, since the overlapping minibands have the same symmetry, $(M_z = 0)$, minigaps instead of an energy continuum are originated.

The differences are enhanced by the magnetic field. As can be seen in Figure 1b, the magnetic field removes spherical degeneracy yielding an energy spectrum where wide $(M_z = 0)$ and narrow $(M_z \neq 0)$ minibands alternate. The shape of the minibands (Figure 1b) is not substantially altered when magnetic fields as high as 20 T are applied, despite that for $B > 10.5$ T the radius of the QD (8 nm) exceeds the magnetic length and, therefore, the effect of the magnetic field exceeds that of spatial confinement. The reason is that the states corresponding to the same M_z evolve in a similar way in the range of laboratory fields, the resulting effect being a parallel shift of the minibands. A linear Zeeman term is, then, responsible for the splitting of $M_z > 0$ minibands that can appear in a previously forbidden region and results in a spectrum that combines narrow $M_z > 0$ quasi-states and broad $M_z = 0$ minibands. This would translate into a spectrum with a mixture of sharp and broad transitions.

A radically different behavior is exhibited by 1D chains of antidots, whose building blocks mainly localize their charge density in the external clad. We have carried out calculations for a 1D chain built of internal core of ZnSe of radius $R = 8$ nm and an external InAs clad of thickness $W = 2$ nm. The internal core acts as a barrier and the external layer, as a well. The conduction band offset is modeled by a 1.26 eV[30] potential barrier. Figure 2 shows the miniband formation at different magnetic fields ($B = 0$, 20, 40 T). Consecutive $M_z = 0$ minibands overcome the gap existing between them, reflecting a nearly semimetallic behavior for $d = 0.1$ nm. If we decrease the interacting distance, new minigaps open at the crossing points. This occurs because successive minibands correspond to the same M_z value, which contrasts with the abovementioned overlap of subsequent minibands of different M_z found in chains of truncated cones and chains of SK islands.[15]

Antidot systems with larger effective masses (ZnS/CdS) and different thickness of the layers exhibited similar qualitative behavior,[44] so that we may conclude that the internal geometry of the dots is the key factor influencing the energy interaction and therefore, the interdot tunneling. Other parameters may, however, enhance these properties, as for example the nature and position of the ground miniband. Thus, for systems with an external clad, large enough to fully localize the wave function, it presents a core-like nature. On the other hand, the larger is the effective mass the stronger the wave function is localized in the region where the dots overlap and, then, the greater is the separation of the ground miniband from the rest of the spectrum.

This very narrow ground miniband, with electronic densities strongly localized along the z-axis, in the region between the dots, is almost unaffected by the magnetic field. However, in the weak coupling regime, the charge is much less localized and the miniband results destabilized by the magnetic field (Figures 2b and 2c). As a result, a change of the ground-state symmetry can be seen, as it has previously been reported for an isolated antidot.[59]

VCQDs with a truncated square-based pyramidal shape have been proposed as good candidates for remaining quantum wires at high temperatures.[15] The reason is that in a low interacting regime (i.e., when the minibands start to converge to the solutions of a single dot) these structures are able to suppress optical phonon scattering which is dominant at high temperatures. This feature is also observed for the same regime when spherical coupled large dots are considered (Figure 1). There, the large minigaps between successive narrow minibands (greater than LO-phonon energy of about 30 meV[9]) prevents the inter and intraminiband scattering.[72] A quantum wire resistant to high temperatures may also be achieved by a chain built of antidots, since it is found that a narrow ground miniband separates from the rest of the spectrum, preventing the scattering (Figure 2a).

3.2. Hole Minibands. In this section we study the hole energy spectra of chains built of uniform and multilayer (antidots) nanocrystals. As expected, the higher effective masses of holes lead to spectra denser than electrons, and the interaction between the heavy and light hole (that, unlike electrons, allow the miniband limits to be found at q values others than 0 and π/D) makes them more complex.

We first present results on chains of antidots because the narrow well-acting clad prevents states of $\tilde{n}Q_F$ with $\tilde{n} > 1$ to appear in the lower part of the spectrum, making it simpler and,

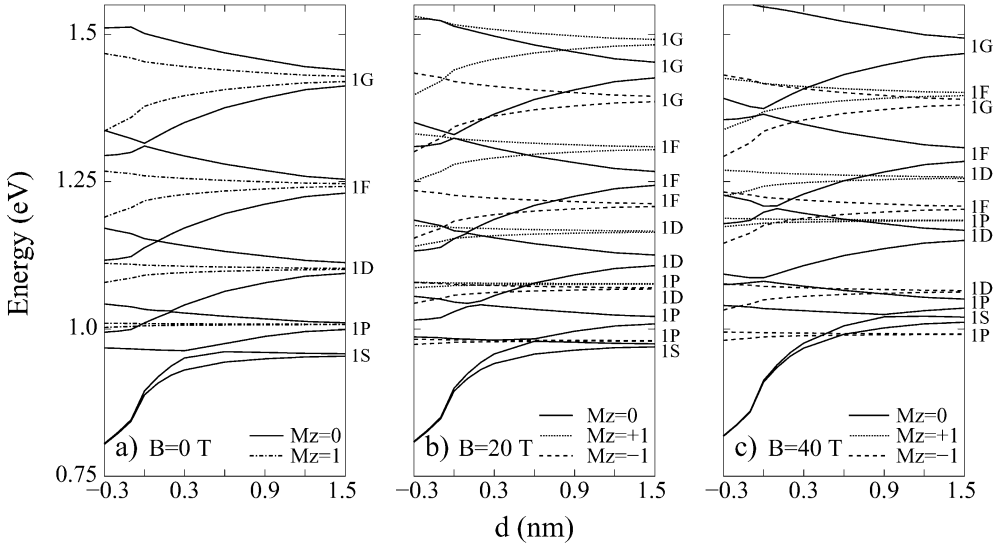

Figure 2. Electron minibands edges corresponding to a 1D array of ZnSe/InAs nanocrystals (ZnSe radius $R = 8$ nm, InAs shell width $W = 2$ nm) vs interdot separation distance d for three values of the axially applied magnetic field: (a) $B = 0$ T; (b) $B = 20$ T; (c) $B = 40$ T. Only $M_z = 0, \pm 1$ minibands are displayed.

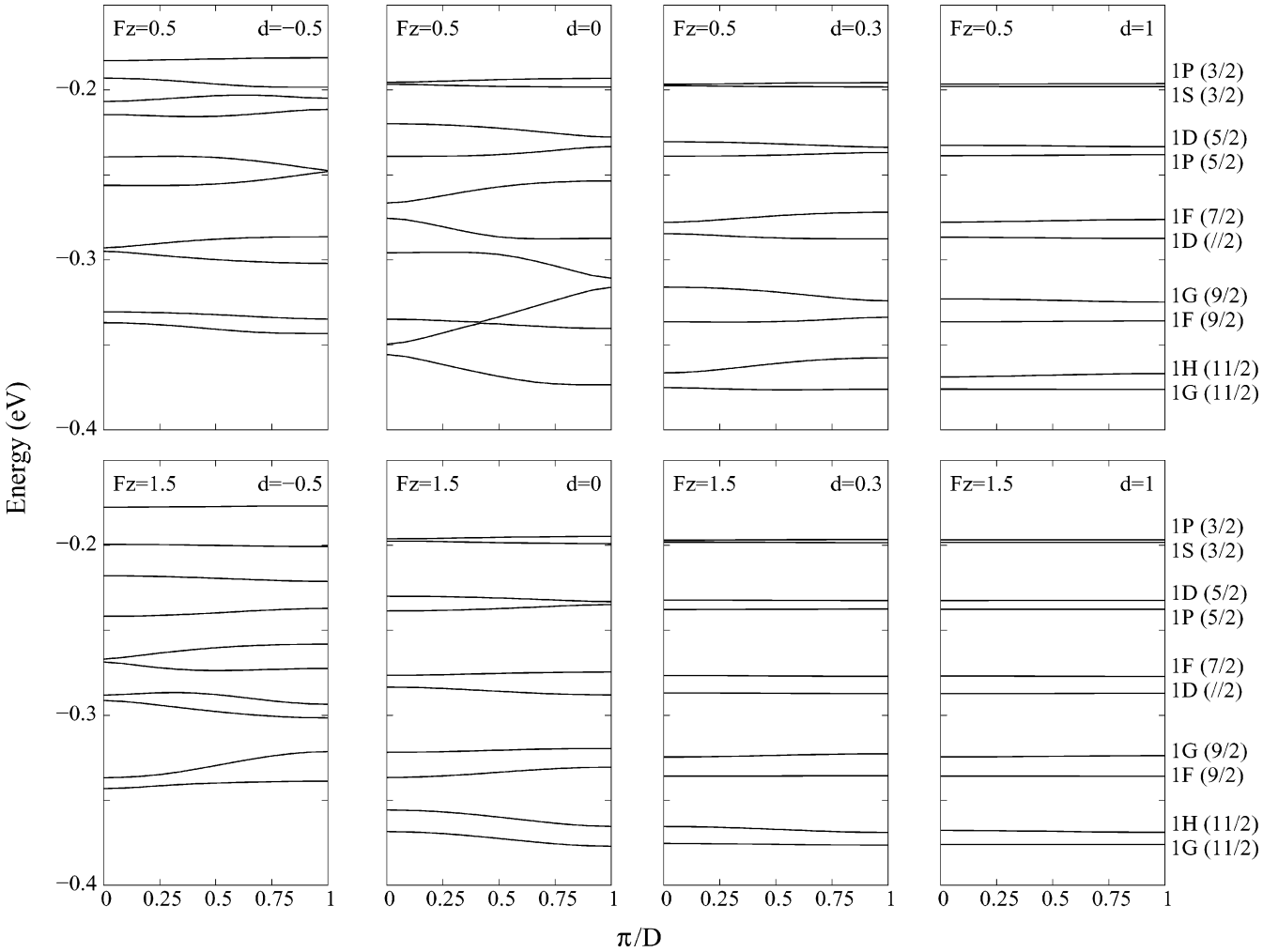

Figure 3. Hole miniband dispersions corresponding to different separation distances d for a chain of ZnSe/InAs nanocrystals ($R = 8$ nm, $W = 2$ nm). $F_z = |0.5|$ and $F_z = |1.5|$ are displayed separately for the sake of clarity. The spherical states notation in the noncoupling regime is included.

additionally, because the interdot interaction, stronger than in chains of homogeneous dots, enhances the studied effects.

The miniband structure of a chain of ZnSe/InAs antidots, with an internal barrier-like ZnSe core of radius $R = 8$ nm and an external well-acting clad of thickness $W = 2$ nm, for several interdot d distances, is presented in Figure 3. The corresponding miniband limits vs distance are plotted in Figure 4. In these calculations, a 0.99 eV ZnSe/InAs band offset[30] is assumed as the potential barrier, and the Luttinger InAs parameters, $\gamma = 8.4$ and $\gamma_1 = 19.7$,[69] are employed for the entire structure.[73]

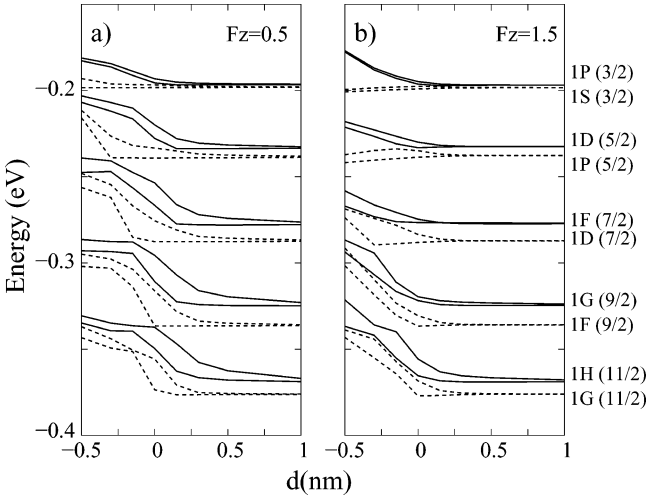

Figure 4. Hole miniband edges vs separation distance d for a ZnSe/InAs chain ($R = 8$ nm, $W = 2$ nm). (a) $F_z = |0.5|$; (b) $F_z = |1.5|$. For each miniband, limits are defined by the same kind of line (solid or dashed).

The polymeric environment of the QDs is modeled by a 4-eV rectangular barrier.

By looking at Figures 2a and 4 we see that the interdot interactions are weaker in holes than in electrons, yielding narrower hole minibands. On the other hand, Figure 3 shows that, as in electrons, the lower is the z-component of the angular momentum, the stronger is the interdot interaction and the wider the miniband. However, as it comes from Figure 4, no big differences in minibandwidth for $F_z = 0.5$ and 1.5 are found, in contrast with the electrons behavior (see Figure 2a). This is related to the fact that hole functions have four components with M_z values $F_z - 3/2$, $F_z - 1/2$, $F_z + 1/2$, $F_z + 3/2$. Thus, states $F_z = 0.5$ and $F_z = 1.5$ have three components with the same M_z and only one with distinct M_z value. Also Figure 3 shows that, as expected, the miniband limits correspond to $q = 0$ and $q = \pi/D$ except when the interdot interaction is strong (i.e., $F_z = 0.5$ and $d \leq 0.3$ nm). Unlike the electrons (see Figures 2a and 4) there is not an interdot distance yielding a quasi continuum hole energy, neither a core-like hole ground miniband that results more and more stabilized as the interaction grows and wider minigaps appear.

To see the influence of geometry and specific properties of the building blocks (effective masses and potentials) we also study chains made of ZnSe/InAs antidots of internal radius $R = 5$ nm and external clad $W = 1$ nm thick, and chains of ZnS/CdS antidots with the same geometries. For the later nanocrystals, a 0.5 eV ZnS/CdS band offset is assumed as the potential barrier, and the Luttinger CdS parameters $\gamma = 0.544$ and $\gamma_1 = 2.012$[69] are employed for the entire structure.

In all studied cases the ground miniband has $F_z = 1.5$ symmetry in the strong interaction regime and $F_z = 0.5$ in the weak interaction regime. The reason for the change of the ground miniband symmetry in the strong and weak interaction regimes may be found in the associated envelope function. This function has four components with well defined M_z, namely $M_z = -1, 0, 1, 2$ if $F_z = 0.5$, and $M_z = 0, 1, 2, 3$ if $F_z = 1.5$. The $M_z = 0, 2$ components show, in these two cases, bonding character, while the other two components show an antibonding character, the always negligible weight of the $M_z = 3$ component being responsible for a greater stabilization of $F_z = 1.5$.

Figure 5 shows the hole band structure in the regime of strong interaction ($d = -0.5$ nm) for the four studied chains. A major difference can be seen: the ground state ($F_z = 1.5$) of both

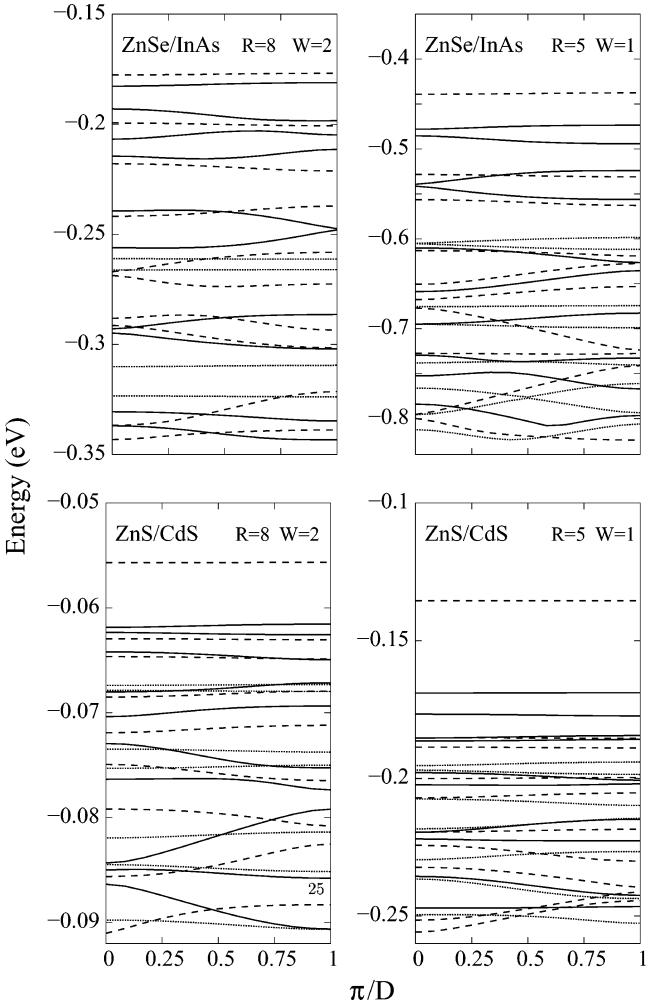

Figure 5. Hole miniband dispersion for d = −0.5 nm of several chains built of antidots with different core/shell materials and clad sizes. Solid, dashed and dotted lines correspond to $F_z = |0.5|$, $F_z = |1.5|$, and $F_z = |2.5|$, respectively.

ZnS/CdS chains separates from the rest of the spectrum when the interaction is strong. This effect is more pronounced if $W = 1$ nm. Indeed, even in the $W = 1$ nm ZnSe/InAs chain one may see some stabilization of the ground-state energy. This effect also appears in the electron spectra, as we have reported in the previous section. However, while in the electron case it is a rather general phenomena, we can see in Figure 5 that, for holes, it is quite sensitive to geometry and intrinsic properties of the building blocks.

Especially relevant is the influence of the magnetic field on the low-lying ZnSe/InAs minibands. As stated above, the low-lying minibands of this chain of antidots do not separate from the rest of spectrum. As a matter of fact, their corresponding hole density distribution shows rather scarce density in the interdot area (see Figures 6a and 6c). The magnetic field concentrates such density distribution in the interdot region, highly enhancing the interdot tunneling (see Figures 6b and 6d).

Finally, we study a chain built of uniform InAs nanocrystals of radius similar to the studied antidots chains ($R = 10$ and $R = 6$ nm). The interaction is negligible in these cases, and no minibands open significantly. Only in chains built of very small uniform InAs nanocrystals ($R = 3$ nm) one can see minibands of width similar to the above-mentioned chains of antidots and also some anticrossings leading the miniband limits to appear at q values others than $q = 0$ and $q = \pi/D$.

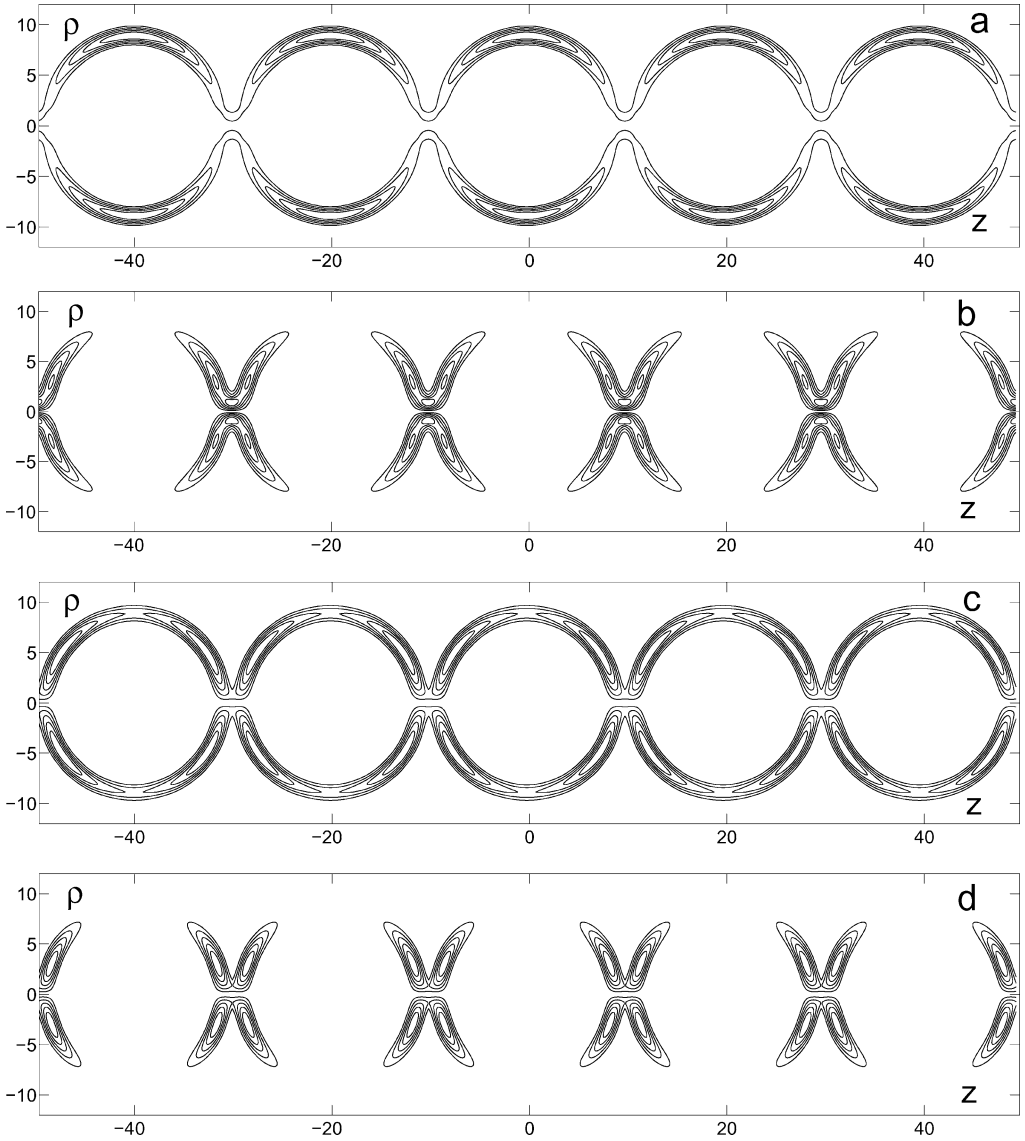

Figure 6. Hole density distribution vs magnetic field of the lowest-lying $F_z = |0.5|$ and $|1.5|$ minibands of an infinite chain built of ZnSe/InAs ($R = 8$ nm, $W = 2$ nm) antidots. (a) Lowest-lying $F_z = |0.5|$ miniband at $B = 0$ T; (b) lowest-lying $F_z = -0.5$ miniband at $B = 40$ T; (c) lowest-lying $F_z = |1.5|$ miniband at $B = 0$ T; (d) lowest-lying $F_z = -1.5$ miniband at $B = 40$ T.

4. Concluding Remarks

The energy structure of the investigated chains, built of spherical nanocrystals, contains sets of minibands of different widths. The width differences are specially important in the electron energy levels of the antidots chain. In this case, the wide, $M_z = 0$, minibands may overcome the minigaps, anticross and open new minigaps as the building blocks get closer. Simultaneously, a very narrow ground miniband separates from the rest of the spectrum. The hole spectra are denser and the differences in the minibandwidth are smaller. Also, in the case of antidot chains, a narrow ground miniband may separate from the rest of the spectrum, more or less, depending on the intrinsic properties of the building blocks. As a result, a strong red-shift in the luminescence should be expected when the nanocrystals are strongly coupled. The magnetic field produces the splitting of minibands of different width (degenerate at $B = 0$) so that narrow minibands are moved toward the energy gaps yielding a sequence of narrow and wide minibands, that would translate into a spectrum with sharp and broad transitions.

Acknowledgment. Financial support from Generalitat Valenciana CTIDIB-2002/189 and UJI-Bancaixa P1-B2002-01 is gratefully acknowledged. Generalitat Valenciana FPI grant (J.D.) is also acknowledged.

References and Notes

(1) Riemann, S. M.; Manninen, M. *Rev. Mod. Phys.* **2002**, *74*, 1283.
(2) Partoens, B.; Peeters, F. M. *Phys. Rev. Lett.* **2000**, *84*, 4433; Partoens, B.; Peeters, F. M. *Europhys. Lett.* **2001**, *56*, 86.
(3) Xie, Q.; Madhukar, A.; Chen, P.; Kobayashi, N. P. *Phys. Rev. Lett.* **1995**, *75*, 2542.
(4) Solomon, G. S.; Trezza, J. A.; Marshall, A. F.; Harris, J. S. *Phys. Rev. Lett.* **1996**, *76*, 952.
(5) Barabási, A. L. *Appl. Phys. Lett.* **1997**, *70*, 764.
(6) Schittenhelm, P.; Engel, C.; Findeis, F.; Abstreiter, G.; Darhuber, A. A.; Bauer, G.; Kosogov, A. O.; Werner, P. *J. Vac. Sci. Technol. B* **1998**, *16*, 1575.
(7) Flebbe, O.; Eisele, H.; Kalka, T.; Heinrichsdorff, F.; Krost, A.; Bimberg, D.; Dähne-Prietsch, M. *J. Vac. Sci. Technol. B* **1999**, *17*, 1639.
(8) Heitz, R.; Kalburge, A.; Xie, Q.; Grundmann, M.; Chen, P.; Holffmann, A.; Madhukar, A. *Phys. Rev. B* **1998**, *57*, 9050.
(9) Grundmann, M.; Stier, O.; Bimberg, D. *Phys. Rev. B* **1995**, *52*, 11969.
(10) Stier, O.; Grundmann, M.; Bimberg, D. *Phys. Rev. B***1999**, *59*, 5688.

(11) Cusak, M. A.; Briddon, P. R.; Jaros, M. *Phys. Rev. B* **1996**, *54*, 2300.
(12) Georgsson, K.; Carlsson, N.; Samuelson, L.; Seifert, W.; Wallenberg, L. R. *Appl. Phys. Lett.* **1995**, *67*, 2981.
(13) Ledentsov, N. N.; Shchukin, V. A.; Grundmann, M. *Phys. Rev. B* **1996**, *54*, 8743.
(14) Pryor, C.; Pistol, M.-E.; Samuelson, L. *Phys. Rev. B* **1997**, *56*, 10404.
(15) Pryor, C. *Phys. Rev. Lett.* **1998**, *80*, 3579.
(16) Wu, W.; Tucker, J. R.; Solomon, G. S.; Harris, J. S. *Appl. Phys. Lett.* **1997**, *71*, 1083.
(17) Szafran, B.; Bednarek, S.; Adamowski, J. *Phys. Rev. B* **2001**, *64*, 125301.
(18) Bayer, M.; Hawrylak, P.; Hinzer, K.; Fafard, S.; Korkusinski, M.; Wasilewski, Z. R.; Stern, O.; Forchel, A. *Science* **2001**, *291*, 451.
(19) Awschalom, D. D.; Loss, D.; Samarth, N. (Eds.) *Semiconductor Spintronics and Quantum Computation*; Springer: Berlin, 2002.
(20) Li, X.-Q.; Yan, Y. *Phys. Rev. B* **2002**, *65*, 205301.
(21) Schomburg, E.; Henini, M.; Chamberlain, J. M.; Steenson, D. P.; Brandl, S.; Hofbeck, K.; Renk, K. F.; Wegscheider, W. *Appl. Phys. Lett.* **1999**, *74*, 2179.
(22) Klappenberger, F.; Ignatov, A. A.; Winnerl, S.; Schomburg, E.; Wegscheider, W.; Renk, K. F. *Appl. Phys. Lett.* **2001**, *78*, 1673.
(23) Jiménez, J. L.; Fonseca, L. R. C.; Brady, D. J.; Leburton, J. P.; Wohlert, D. E.; Cheng, K. Y. *Appl. Phys. Lett.* **1997**, *71*, 3558.
(24) Shoji, H.; Nakata, Y.; Mukai, K.; Sugiyama, Y.; Sugawara, M.; Yokoyama, N.; Ishikawa, H. *Appl. Phys. Lett.* **1997**, *71*, 193.
(25) Sakaki, H. *Jpn. J. Appl. Phys.* **1989**, *28*, L314.
(26) Mews, A.; Eychmüller, A.; Giersig, M.; Schoos, D.; Weller, H. *J. Phys. Chem.* **1994**, *98*, 934.
(27) Alivisatos, A. P. *Nature* **1996**, *271*, 933.
(28) Mews, A.; Kadavanich, A. V.; Banin, U.; Alivisatos, A. P. *Phys. Rev. B* **1996**, *53*, R13242.
(29) Banin, U.; Cao, Y.; Katz, D.; Millo, O. *Nature* **1999**, *400*, 542.
(30) Cao, Y.; Banin, U. *J. Am. Chem. Soc.* **2000**, *122*, 9692.
(31) Millo, O.; Katz, D.; Cao, Y.; Banin, U. *Phys. Rev. Lett.* **2001**, *86*, 5751.
(32) Braun, M.; Burda, C.; El-Sayed, M. A. *J. Phys. Chem. A* **2001**, *105*, 5548.
(33) Mirkin, C. A.; Letsinger, R. L.; Mucic, R. C.; Storhoff, J. J. *Nature* **1996**, *382*, 607.
(34) Alivisatos, A. P.; Johnsson, K. P.; Peng, X.; Wilson, T. E.; Loweth, C. J.; Bruchez, M. P., Jr.; Schultz, P. G. *Nature* **1996**, *382*, 609.
(35) Pileni, M. P. *J. Phys. Chem. B* **2001**, *105*, 3358.
(36) Legrand, J.; Ngo, A. T.; Petit, C.; Pileni, M. P. *Adv. Mater.* **2001**, *13*, 58.
(37) Velev, O. D.; Lenhoff, A. M.; Kaler, E. W. *Science* **2000**, *287*, 2240.
(38) Lin, X. M.; Jaeger, H. M.; Sorensen, C. M.; Klabunde, K. J. *J. Phys. Chem. B* **2001**, *105*, 3353.
(39) Chung, S. W.; Markovich, G.; Heath, J. R. *J. Phys. Chem. B* **1998**, *102*, 6685.
(40) Lin, J.; Zhou, W.; Kumbhar, A.; Wiemann, J.; Fang, J.; Carpenter, E. E.; O'Conor, C. J. *J. Solid State Chem.* **2001**, *159*, 26.
(41) Tatarkova, S. A.; Carruthers, A. E.; Dholakia, K. *Phys. Rev. Lett.* **2002**, *89*, 283901.
(42) Artemyev, M. V.; Bibik, A. I.; Gurinovich, L. I.; Gaponenko, S. V.; Woggon, U. *Phys. Rev. B* **1999**, *60*, 1504.
(43) Döllefeld, H.; Weller, H.; Eychmüller, A. *Nano Lett.* **2001**, *1*, 267.
(44) Díaz, J. G.; Jaskólski, W.; Planelles, J.; Aizpurua, J.; Bryant, G. W. *J. Chem. Phys.* **2003**, *119*, 7484.
(45) Peng, X.; Manna, L.; Yang, W.; Wickham, J.; Scher, E.; Kadavanich, A.; Alivisatos A. P. *Nature* **2000**, *404*, 59.
(46) Jacak, L.; Hawrylak, P.; Wójs, A. *Quantum Dots*; Springer: Berlin, 1998.
(47) Chakraborty, T. *Quantum Dots*; Elsevier: Amsterdam, 1999.
(48) Bylicki, M.; Jaskólski, W. *Phys. Rev. B* **1999**, *60*, 15924.
(49) Jaskólski, W.; Bosek, M.; Bylicki, M.; Planelles, J. *Vacuum* **2001**, *63*, 185.
(50) Lorke, A.; Luyken, R. J.; Govorov, A. O.; Kotthaus, J. P.; García, J. M.; Petroff, P. M. *Phys. Rev. Lett.* **2000**, *84*, 2223.
(51) Lieb, E. H.; Solovej, J. P.; Yngvason, J. *Phys. Rev. B* **1995**, *51*, 10646.
(52) Bimberg, D.; Grundmann, M.; Ledentsov, N. N. *Quantum Dot Heterostructures*; Wiley: Chichester, 2001.
(53) Sadowski, M. L.; Potemski, M.; Gyuberg, M. *Optical Properties of Semiconductor nanostructures*; NATO series vol. 81, Kluwer: Dordrecht, 1999.
(54) Woggon, U. *Optical Properties of Semiconductor Quantum Dots*; Springer-Verlag: Berlin, 1997.
(55) Ando, T.; Arakawa, Y.; Foruka, K.; Komiyama, S.; Nakashima, H.,Eds.; *Mesoscopic Physics and Electronics*; Springer: Berlin, 1998.
(56) Loss, D.; DiVincenzo, D. P. *Phys. Rev. A* **1998**, *57*, 120.
(57) Burkard, G.; Loss, D. *Europhys. News* **2002**, *33*, 166.
(58) Jaskólski, W.; Bryant, G. W.; Planelles, J.; Zielinski, M. *Int. J. Quantum Chem.* **2002**, *90*, 1075.
(59) Planelles, J.; Díaz, J. G.; Climente, J.; Jaskólski, W. *Phys. Rev. B* **2002**, *65*, 245302.
(60) Sercel, P. C.; Vahala, K. J. *Phys. Rev. B* **1990**, *42*, 3690.
(61) Planelles, J.; Jaskólski, J.; Aliaga, J. I. *Phys. Rev. B* **2002**, *65*, 033306.
(62) Planelles, J.; Climente, J.; Díaz, J. G.; Jaskólski, W. *J. Phys. Condens. Matter* **2002**, *14*, 12537.
(63) Efros, Al. L.; Rosen, M. *Phys. Rev. B* **1998**, *58*, 7120.
(64) Planelles, J.; Jaskólski, W. *J. Phys. Condens. Matter* **2003**, *65*, L67−L75.
(65) Arnoldi, W. E. *Q. J. Appl. Math.* **1951**, *9*, 17. Saad, Y. *Numerical Methods for Large Scale Eigenvalue Problems*; Halsted Press: New York, 1991; Morgan, R. B. *Math. Comput.* **1996**, *65*, 1213.
(66) Lehoucq, R. B.; Sorensen, D. C.; Vu, P. A.; Yang, C. *ARPACK: Fortran subroutines for solving large scale eigenvalue problems, Release 2.1*, 1998; Lehoucq, R. B.; Sorensen, D. C.; Yang, C. *ARPACK User's Guide: Solution of Large-Scale Eigenvalue Problems with Implicit Restarted Arnoldi Methods*; SIAM: Philadelphia, 1998.
(67) Li, Y.; Voskoboynikov, O.; Lee, C. P.; Sze, S. M. *Solid State Commun.* **2001**, *120*, 79.
(68) Li, Y.; Voskoboynikov, O.; Lee, C. P.; Sze, S. M. *Comput. Phys. Commun.* **2001**, *141*, 66.
(69) Madelung, O., Landolt-Börstein, Eds.; *Numerical Data and Functional Relationships in Science and Technology*; Springer-Verlag: Berlin.
(70) Note that the presence of inversion symmetry in the sphere would suppress the piezoelectric splitting if eventually strained spheres were considered.
(71) Some lines in the figure do not look smooth because we have made calculations for eight discrete vaues of the interdot distance *d* and plotted the lines connecting them.
(72) This miniband structure may also be favorable for generating Bloch oscillations because damping attributed to optical phonon scattering has been suppressed.[14]
(73) Axial approximation could be used for a Hamiltonian in cylindrical coordinates. However, for a more adequate comparison with results of isolated nanocrystals, the so-called spherical approximation with only two Luttinger parameters is employed in all cases.